Korea-Australia Rheology Journal
Vol. 17, No. 3, September 2005 pp. 99-110

Finite element analysis of viscoelastic flows in a domain with geometric singularities

Sungho Yoon and Youngdon Kwon*
School of Applied Chemistry and Chemical Engineering, Sungkyunkwan University, Suwon, Kyunggi-do 440-746, Korea
(Received June 15, 2005)

Abstract

This work presents results of finite element analysis of isothermal incompressible creeping viscoelastic flows with the tensor-logarithmic formulation of the Leonov model especially for the planar geometry with singular corners in the domain. In the case of 4:1 contraction flow, for all 5 meshes we have obtained solutions over the Deborah number of 100, even though there exists slight decrease of convergence limit as the mesh becomes finer. From this analysis, singular behavior of the corner vortex has been clearly seen and proper interpolation of variables in terms of the logarithmic transformation is demonstrated. Solutions of 4:1:4 contraction/expansion flow are also presented, where there exists 2 singular corners. 5 different types spatial resolutions are also employed, in which convergent solutions are obtained over the Deborah number of 10. Although the convergence limit is rather low in comparison with the result of the contraction flow, the results presented herein seem to be the only numerical outcome available for this flow type. As the flow rate increases, the upstream vortex increases, but the downstream vortex decreases in their size. In addition, peculiar deflection of the streamlines near the exit corner has been found. When the spatial resolution is fine enough and the Deborah number is high, small lip vortex just before the exit corner has been observed. It seems to occur due to abrupt expansion of the elastic liquid through the constriction exit that accompanies sudden relaxation of elastic deformation.

Keywords : high Deborah number, tensor-logarithm, stability, Leonov model, contraction flow, constriction flow

1. Introduction

In high Deborah number flows, numerical modeling of viscoelastic flow in a domain with sharp corners or geometric singularities has been a formidable task in the field of computational non-Newtonian fluid dynamics. Its difficulty may be expressed via improper mesh convergence, solution inaccuracy and violation of positive definiteness of the conformation tensor (violation of strong ellipticity of partial differential equations), which ultimately result in degradation of the whole numerical scheme. Recently a new formalism of existing constitutive equations has been suggested by Fattal and Kupferman (2004), which forbids violation of positive definiteness of the conformation tensor simply employing logarithmic transform. In the current authors' opinion, it may be quite a breakthrough that possibly reveals undiscovered area of solutions in computation of high Deborah number viscoelastic flows.

The first finite element implementation of this new formalism has been performed by Hulsen and coworkers (2005), who have demonstrated dramatic stabilization of the numerical procedure as long as proper viscoelastic constitutive equations are included. Whereas they clearly demonstrate the potential of the new formulation in modeling of viscoelastic flow past a cylinder, Kwon (2004) has given a numerical result of the flow modeling in the domain with a sharp corner. In comparison with the conventional method, stable computation has been demonstrated even in this flow domain with a sharp corner. In the paper (Kwon, 2004), it has been concluded that this new method may work only for constitutive equations proven globally stable. Thus as a result, the stability constraint has to be taken into serious consideration.

Almost no computational result regarding the viscoelastic flow through contraction-expansion (or constriction) pipe has been reported probably due to much higher numerical obstacle present in the flow domain. Within authors' knowledge, computational results only for the flow with rounded corners are currently available, and one example can be found in the work by Szabo and coworkers (1997).

In this work, we first complement the result for the flow through 4:1 planar contraction presented by Kwon (2004) employing finer spatial discretization. Then the viscoelastic flow through 4:1:4 constriction is considered and we make an attempt to verify difficulty that seems more intense than

*Corresponding author: kwon@skku.edu

the complication in the contraction flow. All the results are obtained in isothermal inertialess steady planar viscoelastic flow. As a viscoelastic field equation the Leonov model is chosen, of which the mathematical stability has been proven (Kwon and Leonov, 1995) and the tensor-logarithmic formulation in the 2D planar case is given in Kwon (2004).

2. Equations in 2D planar flow

The differential viscoelastic constitutive equations derived by Leonov (1976) can be written into the following quite general form:

$$\frac{d\boldsymbol{c}}{dt}-\nabla\boldsymbol{v}^T\cdot\boldsymbol{c}-\boldsymbol{c}\cdot\nabla\boldsymbol{v}+\frac{1}{2\theta}\left(\frac{I_1}{I_2}\right)^m\left(\boldsymbol{c}^2+\frac{I_2-I_1}{3}\boldsymbol{c}-\delta\right)=\boldsymbol{0},$$

$$\tau=G\left(\frac{I_1}{3}\right)^n\boldsymbol{c},\qquad W=\frac{3G}{2(n+1)}\left[\left(\frac{I_1}{3}\right)^{n+1}-1\right]. \tag{1}$$

Here $\boldsymbol{c}$ is the elastic Finger strain tensor that describes the accumulated elastic strain in the Finger measure during flow, $\boldsymbol{v}$ is the velocity, $\frac{d\boldsymbol{c}}{dt}=\frac{\partial\boldsymbol{c}}{\partial t}+\boldsymbol{v}\cdot\nabla\boldsymbol{c}$ is the total time derivative of $\boldsymbol{c}$, ∇ is the usual gradient operator in tensor calculus, $\frac{d\boldsymbol{c}}{dt}-\nabla\boldsymbol{v}^T\cdot\boldsymbol{c}-\boldsymbol{c}\cdot\nabla\boldsymbol{v}$ is the upper convected time derivative, G is the modulus and θ is the relaxation time. The tensor $\boldsymbol{c}$ reduces to the unit tensor δ in the rest state and this condition also serves as the initial condition in the start-up flow situation. In the asymptotic limit of $\theta\to\infty$ where the material exhibits purely elastic behavior, it becomes the total Finger strain tensor.

$I_1=\mathrm{tr}\boldsymbol{c}$ and $I_2=\mathrm{tr}\boldsymbol{c}^{-1}$ are the basic first and second invariants of $\boldsymbol{c}$, respectively, and they coincide in planar flows. Due to the characteristic of the Leonov model, the third invariant I_3 satisfies specific incompressibility condition such as $I_3=\det\boldsymbol{c}=1$. In order to rigorously examine the computational robustness of the formulation we do not include any retardation (Newtonian viscous) term that bestows stabilizing effect on the numerical scheme by augmenting the elliptic character in equations of motion. It is well known that the computation without the Newtonian term included in the set of equations becomes quite difficult and easily prone to numerical deterioration. In addition, its absence keeps fast explicit time-marching algorithm for the evolution equations of $\boldsymbol{c}$ from being implemented. Thus the stress relation in Eq.(1) imposes the most stringent condition upon the computation scheme, and we have to apply a conventional Newton-Raphson iteration solver to deal with nonlinear equations. The extra-stress tensor is obtained from the elastic potential W based on the Murnaghan's relation. Since the extra-stress is invariant under the addition of arbitrary isotropic terms, when we present our numerical results we use $\tau=G\left(\frac{I_1}{3}\right)^n(\boldsymbol{c}-\delta)$ instead in order to set 0 for the stress in the rest state. In addition to the linear viscoelastic parameters, it contains 2 nonlinear constants m and n, which can be determined from simple shear and uniaxial extensional flow experiments. The value of the parameter m does not have any effect on the flow characteristics in 2D situation, since two invariants are identical.

The total set of equations in the finite element modeling is composed of Eq.(1) and the following equations of motion and continuity:

$$-\nabla p+\nabla\cdot\tau+2\eta_a\nabla\cdot(\boldsymbol{e}-\bar{\boldsymbol{e}})=\boldsymbol{0},\quad \nabla\cdot\boldsymbol{v}=0. \tag{2}$$

Here p is the pressure, $\boldsymbol{e}=\frac{1}{2}(\nabla\boldsymbol{v}+\nabla\boldsymbol{v}^T)$ is the strain rate tensor, and $\bar{\boldsymbol{e}}$ is its unknown variable for the DEVSS (discrete elastic-viscous split stress) implementation (Guénette and Fortin, 1995). η_a is the parameter with the dimension of viscosity for the DEVSS method, the value of which is set to be identical with that of the zero-shear viscosity $\eta_0=G\theta$ and is raised to augment the stability of the numerical scheme in a few cases.

The essential idea presented by Fattal and Kupferman (2004) in reformulating the constitutive equations is the tensor-logarithmic transformation of $\boldsymbol{c}$ as follows:

$$\boldsymbol{h}=\log\boldsymbol{c}. \tag{3}$$

Here the logarithm operates as the isotropic tensor function, which implies the identical set of principal axes for both $\boldsymbol{c}$ and $\boldsymbol{h}$. In the case of the Leonov model, this $\boldsymbol{h}$ becomes another measure of elastic strain, that is, twice the Hencky elastic strain. While $\boldsymbol{c}$ becomes δ, $\boldsymbol{h}$ reduces to $\boldsymbol{0}$ in the rest state.

In the case of 2D planar flow, the final set of the Leonov constitutive equations in the $\boldsymbol{h}$-form has been obtained in Kwon (2004) as follows:

$$\begin{aligned}&\frac{\partial h_{11}}{\partial t}+v_1\frac{\partial h_{11}}{\partial x_1}+v_2\frac{\partial h_{11}}{\partial x_2}-\frac{2}{h^2}\left(h_{11}^2+h_{12}^2h\frac{e^h+e^{-h}}{e^h-e^{-h}}\right)\frac{\partial v_1}{\partial x_1}\\&\quad-h_{12}\left[\frac{h_{11}}{h^2}\left(1-h\frac{e^h+e^{-h}}{e^h-e^{-h}}\right)+1\right]\frac{\partial v_1}{\partial x_2}\\&\quad-h_{12}\left[\frac{h_{11}}{h^2}\left(1-h\frac{e^h+e^{-h}}{e^h-e^{-h}}\right)-1\right]\frac{\partial v_2}{\partial x_1}\\&\quad+\frac{1}{\theta}\frac{e^h-e^{-h}}{2h}h_{11}=0,\end{aligned}$$

$$\begin{aligned}&\frac{\partial h_{12}}{\partial t}+v_1\frac{\partial h_{12}}{\partial x_1}+v_2\frac{\partial h_{12}}{\partial x_2}-\frac{2h_{11}h_{12}}{h^2}\left(1-h\frac{e^h+e^{-h}}{e^h-e^{-h}}\right)\frac{\partial v_1}{\partial x_1}\\&\quad-\left[\frac{1}{h^2}\left(h_{12}^2+h_{11}^2h\frac{e^h+e^{-h}}{e^h-e^{-h}}\right)-h_{11}\right]\frac{\partial v_1}{\partial x_2}\\&\quad-\left[\frac{1}{h^2}\left(h_{12}^2+h_{11}^2h\frac{e^h+e^{-h}}{e^h-e^{-h}}\right)+h_{11}\right]\frac{\partial v_2}{\partial x_1}\end{aligned}$$

$$+\frac{1}{\theta}\frac{e^{h}-e^{-h}}{2h}h_{12}=0. \quad (4)$$

Here $h=\sqrt{h_{11}^{2}+h_{12}^{2}}$ is the eigenvalue of $\boldsymbol{h}$. Actually the total set of eigenvalues in this 2D flow are h, $-h$ and 0. Together with the equations of continuity and motion, Eqs.(4) constitute a complete set to describe isothermal incompressible planar viscoelastic flow. However due to the form presented in Eqs.(4), artificial numerical difficulty may arise. In addition to the case of rest state, during flow vanishing of the eigenvalue h (it means $\boldsymbol{h}=\boldsymbol{0}$) may occur locally, e.g. along the centerline in the fully developed Poiseuille flow through a straight pipe. Then the coefficients of $\frac{\partial v_i}{\partial x_j}$ and h_{ij} become apparently indeterminate. However proper introduction of asymptotic relation for vanishing h results in

$$\frac{\partial h_{11}}{\partial t}+v_1\frac{\partial h_{11}}{\partial x_1}+v_2\frac{\partial h_{11}}{\partial x_2}-2\frac{\partial v_1}{\partial x_1}-h_{12}\frac{\partial v_1}{\partial x_2}+h_{12}\frac{\partial v_2}{\partial x_1}+\frac{1}{\theta}h_{11}\approx 0,$$

$$\frac{\partial h_{12}}{\partial t}+v_1\frac{\partial h_{12}}{\partial x_1}+v_2\frac{\partial h_{12}}{\partial x_2}-(1-h_{11})\frac{\partial v_1}{\partial x_2}-(1+h_{11})\frac{\partial v_2}{\partial x_1}+\frac{1}{\theta}h_{12}\approx 0,$$

when $h\approx 0$. (5)

These Leonov equations contain one essential feature in incompressible flows: $\det\boldsymbol{c}=1$. (6)
In 2D it reduces to $c_{11}c_{22}-c_{12}^{2}=1$. This incompressibility relation (6) in the notation of the $\boldsymbol{h}$ tensor becomes

$$\mathrm{tr}\boldsymbol{h}=0. \quad (7)$$

It gives another advantage in computation. For example, in 3D due to $h_{11}+h_{22}+h_{33}=0$ one can eliminate one variable (and accordingly one equation) from the set of governing equations. In this 2D analysis, we remove h_{22} from the set, and thus the viscoelastic constitutive equations add only 2 supplementary unknowns such as h_{11} and h_{12}. Based on our numerical scheme explained afterwards, the computation time has diminished to a half.

3. Numerical procedure

We first investigate planar 4:1 abrupt contraction flow with centerline symmetry. The flow geometry and boundary conditions are the same with those employed in Kwon (2004) and again illustrated in Fig. 1. We also solve the problem of planar 4:1:4 constriction or contraction/expansion flow, the problem domain of which is shown in Fig. 2. For both problems, we apply no-slip boundary condition at the wall $\partial\Omega_1$ and specify symmetric natural boundary on the centerline $\partial\Omega_3$. To remove indeterminacy of pressure, we also set the pressure variable as 0 at the exit wall. Fully developed flow conditions are applied for the velocity and $\boldsymbol{h}$ tensor at the inlet $\partial\Omega_4$ but only for the velocity at the outlet $\partial\Omega_2$.

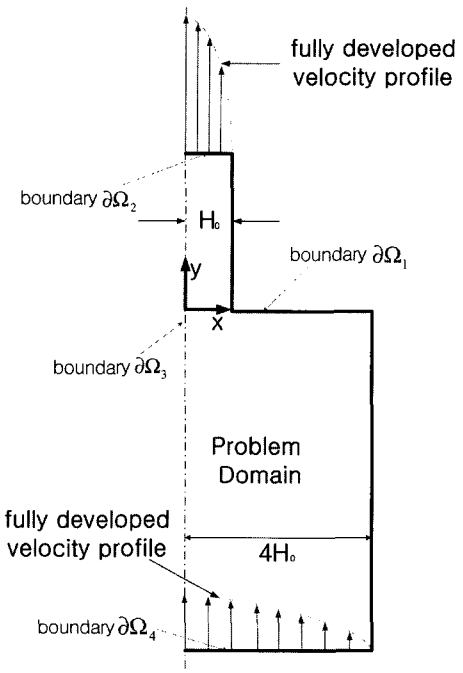

Fig. 1. Problem domain and boundary conditions of the 4:1 contraction flow problem.

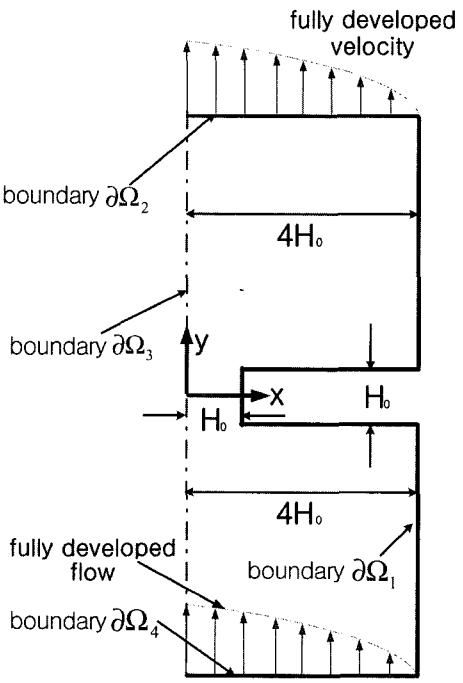

Fig. 2. Problem domain and boundary conditions of the 4:1:4 contraction/expansion flow problem.

When we denote the half width of the narrow channels as H_0, we set the length of the downstream channel as $15H_0$ and the length of the reservoir as $20H_0$ for the contraction flow. For the constriction flow, we set the lengths of both entrance and exit pipes as $14.5H_0$ and the length of con-

striction as H_0. Even though the downstream channel length seems to be rather short to achieve fully developed flow especially for the contraction flow, in order to alleviate computational burden we simply choose this flow geometry.

Whereas the domain of the contraction flow contains only 1 singular point, i.e. the contraction corner, there exits 2 singular points in the constriction problem such as contraction and expansion corners. Thus one can presume that the constriction flow problem may become much harder to solve than that of the contraction flow, and later we present an evidence of this simple conjecture.

With the standard Galerkin formulation adopted as basic computational framework, streamline-upwind/Petrov-Galerkin (SUPG) method as well as discrete elastic viscous stress splitting (DEVSS) algorithm is implemented in order to build relatively robust numerical scheme at high Deborah number flows. The upwinding algorithm developed by Gupta (1997) has been applied. The SUPG scheme is consistent and endows a second order accuracy.

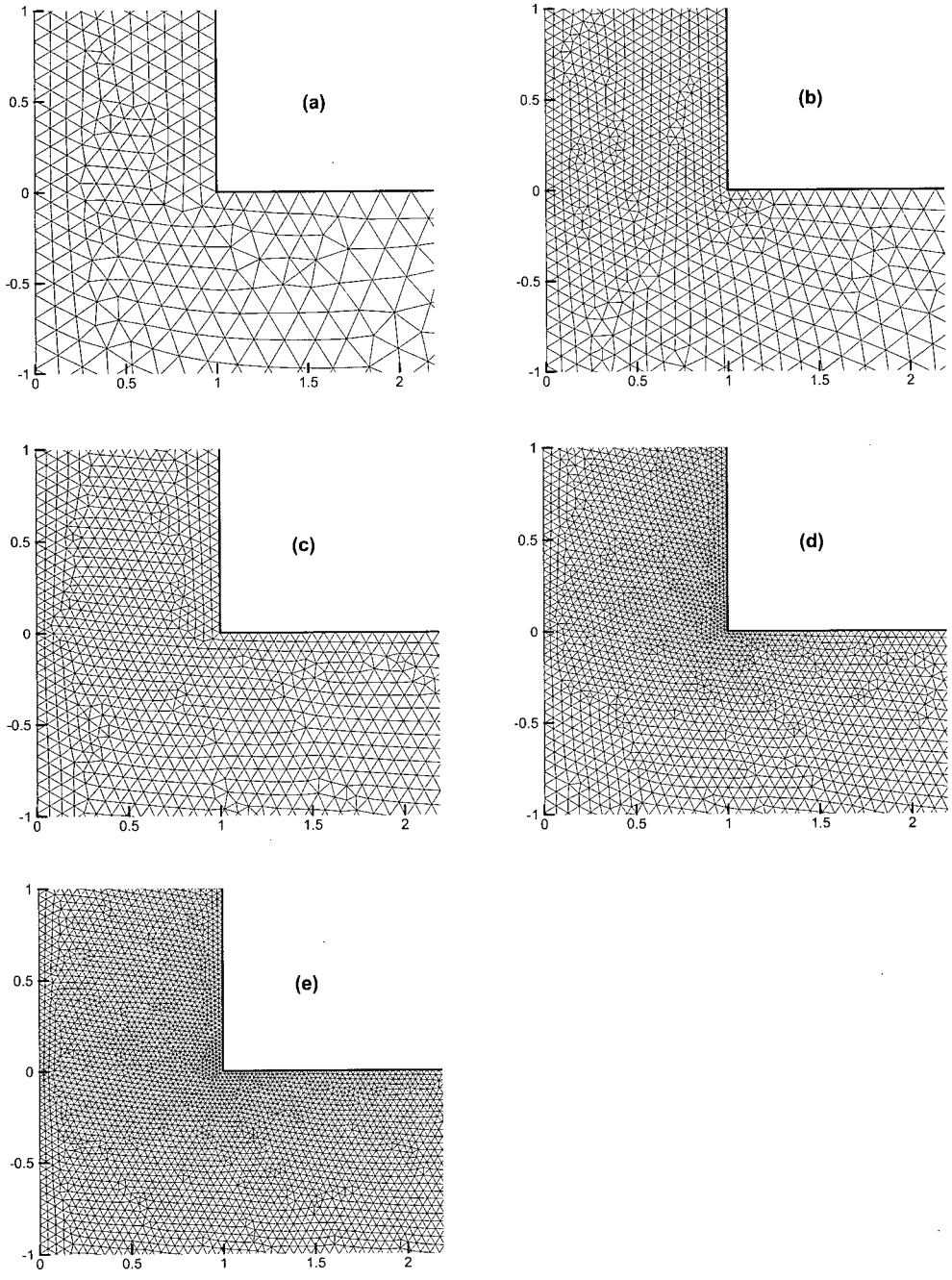

Fig. 3. Partial view of the 5 meshes employed in the analysis of 4:1 contraction flow. (a) Mesh-A1, (b) Mesh-A2, (c) Mesh-A3, (d) Mesh-A4, (e) Mesh-A5.

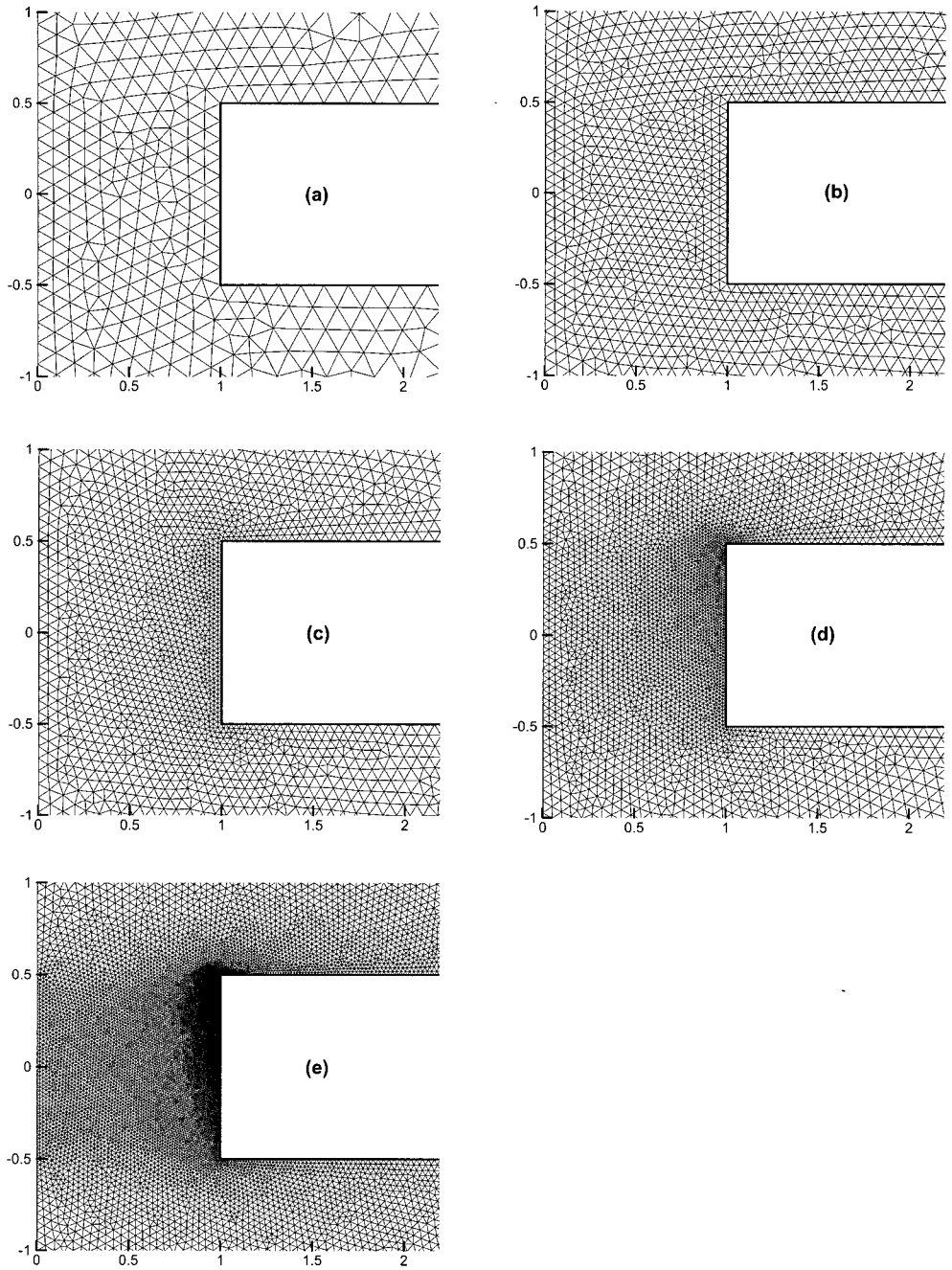

Fig. 4. Partial view of the 5 meshes employed in the analysis of 4:1:4 contraction/expansion flow. (a) Mesh-B1, (b) Mesh-B2, (c) Mesh-B3, (d) Mesh-B4, (e) Mesh-B5.

Table 1. Characteristics of the 5 meshes employed for the analysis of 4:1 contraction flow

	Length of the side of the smallest element	No. of elements	No. of linear nodes	No. of quadratic nodes	No. of unknowns
Mesh-A1	$0.1H_0$	3,491	1,920	7,330	37,000
Mesh-A2	$0.05H_0$	7,174	3,835	14,843	74,712
Mesh-A3	$0.05H_0$	10,679	5,614	21,906	110,080
Mesh-A4	$0.02H_0$	17,393	9,072	35,536	178,432
Mesh-A5	$0.02H_0$	26,181	13,527	53,234	267,044

Table 2. Characteristics of the 5 meshes employed for the analysis of 4:1:4 contraction/expansion flow

	Length of the side of the smallest element	No. of elements	No. of linear nodes	No. of quadratic nodes	No. of unknowns
Mesh-B1	$0.1H_0$	4,262	2,277	8,815	44,368
Mesh-B2	$0.05H_0$	12,254	6,377	25,007	125,536
Mesh-B3	$0.025H_0$	13,966	7,252	28,469	142,884
Mesh-B4	$0.01H_0$	18,271	9,440	37,150	186,360
Mesh-B5	$0.005H_0$	35,673	18,269	72,210	361,916

5 types of meshes are employed for the computation of contraction and constriction flows, respectively, and they are illustrated in Figs. 3 and 4. Corresponding mesh details are given in Tables 1 and 2. Especially for Mesh-B4 and Mesh-B5, the region of exit corner is spatially more refined for detailed analysis of solutions near the corner, and the reason of this asymmetric refinement will become clear when we examine the solutions in the next section.

Linear for pressure and strain rate and quadratic interpolation for velocity and $\boldsymbol{h}$-tensor are applied for spatial continuation of the variables. In this work, we only consider steady inertialess flow of the isothermal incompressible liquid. In order to mimic dimensionless formulation, we simply assign unit values for G and θ and adjust the Deborah number by the variation of the average flow rate. The Deborah number in this contraction or constriction flow is usually defined as

$$De \equiv \frac{U\theta}{H_0}, \tag{8}$$

where U is the average velocity of the liquid in the narrow channel. Also $n = 0.1$ is set to guarantee the mathematical stability even in stress predefined flow history (Kwon and Leonov, 1995) (e.g. in the situation where one assigns traction boundary conditions at the inlet and outlet).

In order to solve the large nonlinear system of equations introduced, the Newton iteration is used in linearizing the system. As an estimation measure to determine the solution convergence, the L_∞ norm scaled with the maximum value in the computational domain is employed. Hence when the variation of each nodal variable in the Newton iteration does not exceed 10^{-4} of its value in the previous iteration, the algorithm concludes that the converged solution is attained. For the viscoelastic variables, we examine the relative error in terms of the eigenvalue of the $\boldsymbol{c}$-tensor. We have found that this convergence criterion imposes less stringent condition on the computational procedure, and it seems quite practical and appropriate since we mainly observe the results in terms of physically meaningful $\boldsymbol{c}$-tensor or stress rather than $\boldsymbol{h}$.

4. Results and discussion

The convergence limits in the scale of the Deborah number are listed in Table 3 for the contraction flow and in Table 4 for the constriction flow, respectively. Both cases exhibit initial increase and then slow decrease in the convergence limit as the spatial discretization becomes refined. From this observation, we may conclude that the numerical scheme still deteriorates as the mesh becomes finer, which may contradict the conclusion assumed in the paper (Hulsen, 2004; Hulsen *et al.*, 2005). However the fact that involving no Newtonian term employed in this study imposes very stringent condition in computation has to be kept in mind. The formulation including the small Newtonian viscous stress significantly stabilize the process, even though we do not report any result in this regard, and we can obtain stable result at the Deborah number as high as several hundreds for all 5 meshes in the contraction flow. We have also found that due to intense nonlinearity present in the $\boldsymbol{h}$-formulation (4) the numerical convergence is quite sensitive to the linearization procedure, and thus determination of accurate convergence limit is rather difficult.

Table 3. Limit of convergence in Deborah number achievable for each mesh types under the SUPG method in 4:1 contraction flow

Mesh-A1	132
Mesh-A2	193
Mesh-A3	169
Mesh-A4	123
Mesh-A5	117

Table 4. Limit of convergence in Deborah number achievable for each mesh types under the SUPG method in 4:1:4 contraction/expansion flow

Mesh-B1	17
Mesh-B2	26
Mesh-B3	23
Mesh-B4	16
Mesh-B5	>10

For the 4:1:4 constriction as well as the 4:1 contraction flow, with the result herein we have not been able to reach the ultimate limit of numerical convergence when the mesh becomes extremely fine. If such a value exists, the numer-

ical degradation may imply important physical meaning such as real instability of any possible kind.

For the constriction flow modeling, the convergence limit in the case of Mesh-B5 is not attained due to heavy computational burden required for its verification. At least, we can assert that the limit is higher than 10 in the Deborah number. Especially for this mesh, the value of $\eta_a = 3.2\eta_0$ is applied due to some difficulty in convergence, even though $\eta_a = \eta_0$ is used for all the other computations. The effect of the variation of η_a has been discussed in detail by Fan *et al.* (1999). In this numerical study, we have found some peculiar flow pattern near the expansion corner, and Mesh-B5 is employed only to confirm this rather uncertain phenomenon. The overall convergence limit is quite low in comparison with the result for the contraction flow. Later, the origin of this difficulty in numerical convergence will be discussed. Irrespective of this rather low convergence limit, the study may provide valuable information in viscoelastic fluid dynamics, since within authors' knowledge there exists no computational result on the abrupt constriction flow modeling. However one can find results on the analysis of viscoelastic constriction flow with corner rounding (Szabo *et al.*, 1997).

Fig. 5 shows streamlines of the contraction flow at $De = 100$ for Mesh-A1, Mesh-A3 and Mesh-A5, respectively, which exhibit large corner vortex. The overall shapes are almost identical, which explains proper mesh convergence in the solution. However one can observe

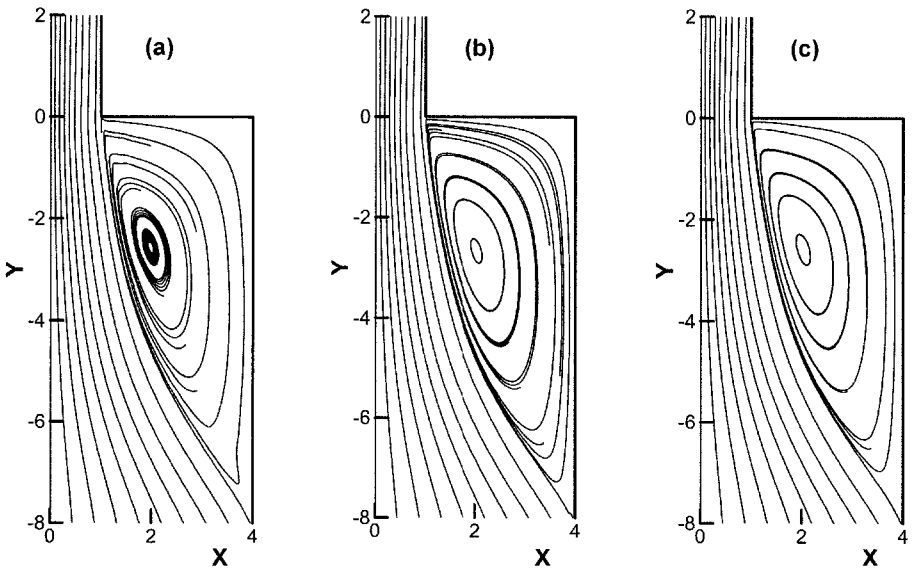

Fig. 5. Streamlines of 4:1 contraction flow at $De = 100$ for (a) Mesh-A1, (b) Mesh-A3 and (c) Mesh-A5.

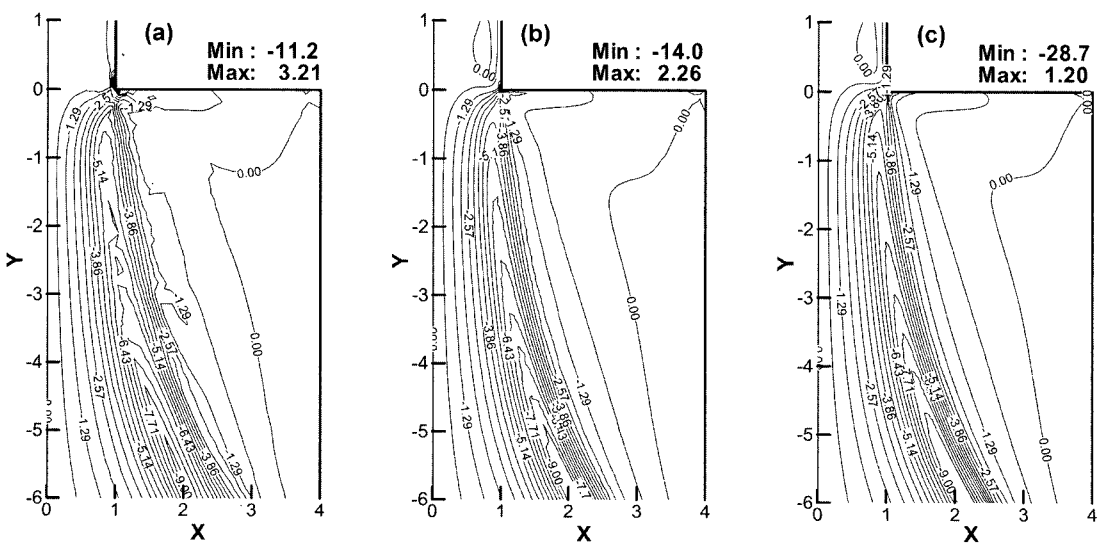

Fig. 6. Shear stress (τ_{xy}) contourlines of 4:1 contraction flow at $De = 100$ for (a) Mesh-A1, (b) Mesh-A3 and (c) Mesh-A5.

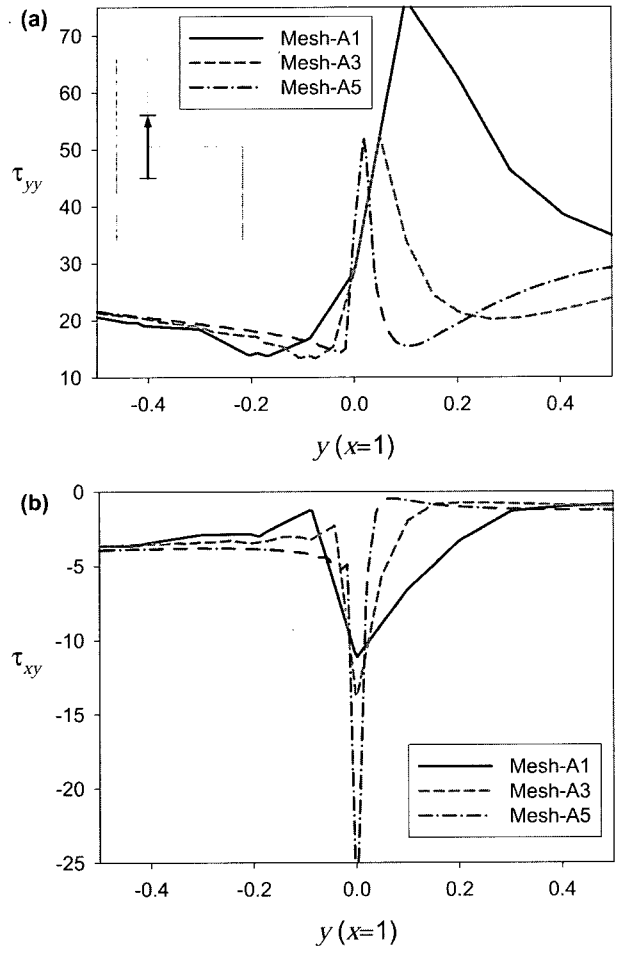

Fig. 7. Stress profiles along the line of $x = 1$ in the 4:1 contraction flow at $De = 100$: (a) the normal stress τ_{yy} in the flow direction, (b) shear stress τ_{xy}.

slight increase of the vortex size with mesh refinement and this characteristic of the solution has been already mentioned previously (Kwon, 2004). Fig. 6 illustrates shear stress contour for the same meshes. High gradient of shear stress near the corner can be noticed and quite stiff variation across the vortex boundary is also found.

In Fig. 7 the stress profiles are shown as functions of y (the flow direction) at $x = 1$ (scaled with H_0). Thus at $y = 0$ they change their domain from the liquid to the solid wall, and the position in $0 \le y$ means the location at the downstream wall. The sharp variation of stresses clearly demonstrates singular behavior of the solutions incurred by the contraction corner. Here we do not observe fluctuation of stress variables along the wall, which have been frequently examined in many publications. This disappearance of numerical artifacts seems to result from the upwinding employed in the computational algorithm. We can examine tendency that the peaks of the stress variables near the corner ($y \approx 0$) become sharper as the mesh becomes finer, and it again suggests appropriate mesh convergence of the solutions.

In the case of finest spatial discretization (Mesh-A5), the normal stresses and the elastic potential have been depicted in Fig. 8. Again one can explicitly see high solution gradient near the corner. In addition, along the centerline gradual increase of the normal stress (τ_{yy}) and elastic potential up to the contraction is also observed, which implies strong extensional deformation of the fluid element in this contraction flow. In the region of vortex, the variation of solutions is rather weak. Fig. 8c specifically illustrates accumulation of the elastic energy near contraction that is partially relaxed along the downstream channel.

Fig. 9 shows streamlines of the constriction flow at

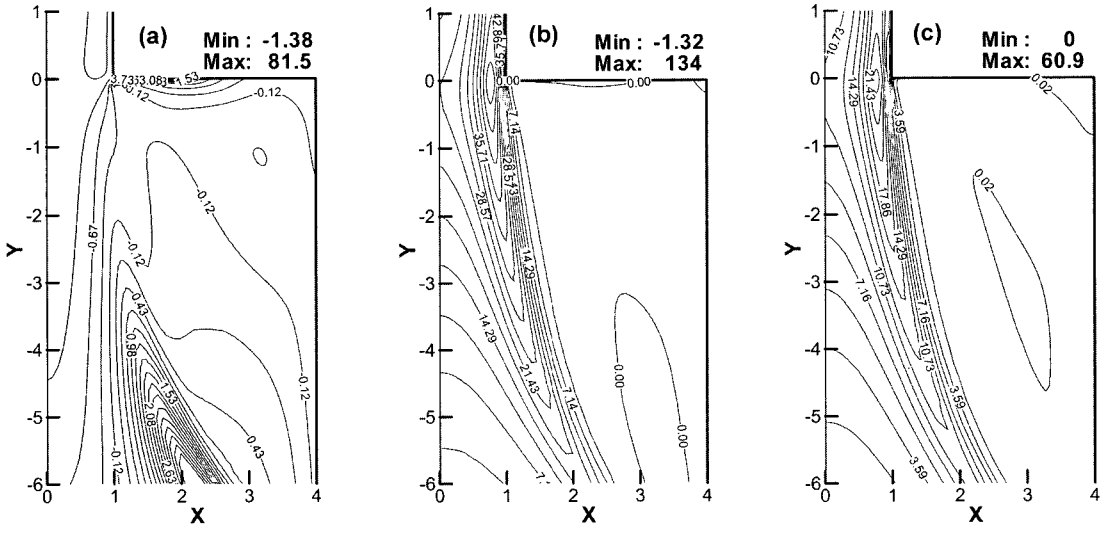

Fig. 8. Normal stress contourlines (a) in the transverse direction (τ_{xx}), (b) in the flow direction (τ_{yy}) and (c) elastic potential W of 4:1 contraction flow at $De = 100$ for Mesh-A5.

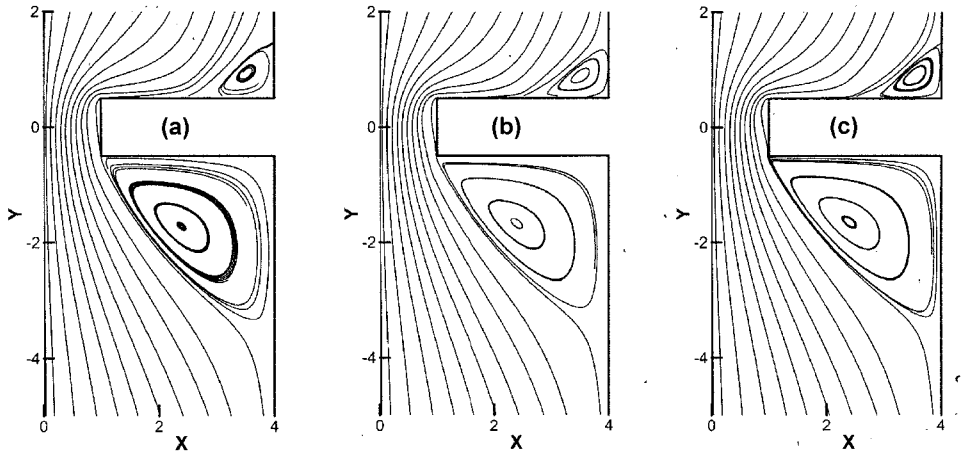

Fig. 9. Streamlines of 4:1:4 constriction flow at $De = 10$ for (a) Mesh-B1, (b) Mesh-B3 and (c) Mesh-B5.

$De = 10$ for Mesh-B1, Mesh-B3 and Mesh-B5, respectively, which exhibit large entrance (upstream) corner vortex but small expansion (downstream) corner vortex. One can hardly notice the difference among the solutions of different meshes and thus Fig. 9 indirectly proves proper mesh convergence with spatial discretization. In all 3 figures, one can find peculiar streamline deflection near the expansion corner. Such deflection seems to be caused by sudden elastic expansion of the liquid at the exit of the narrow channel and it will be further examined in detail later.

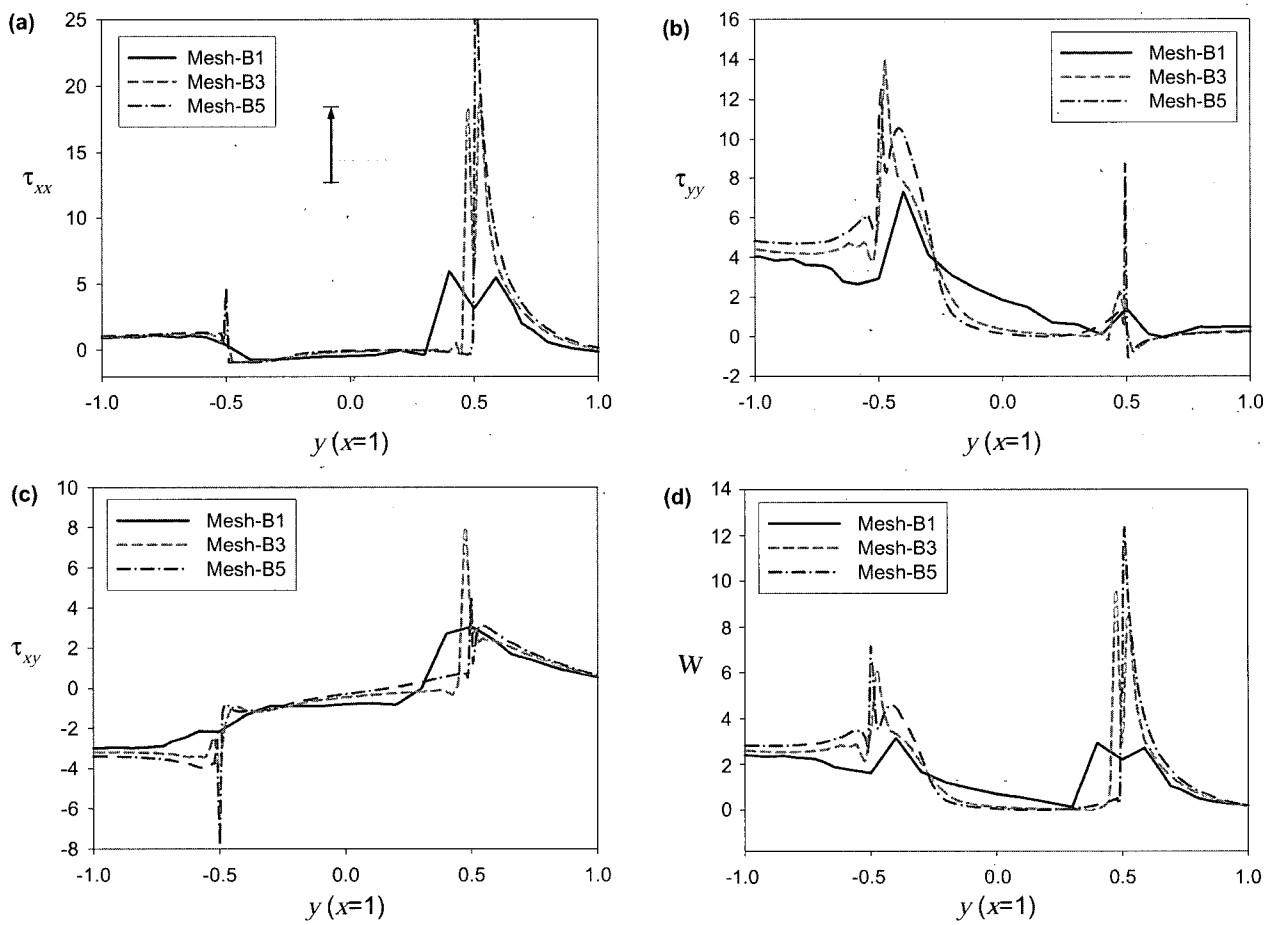

Fig. 10. Variation of the variables along the line of $x = 1$ in the 4:1:4 constriction flow at $De = 10$: (a) the normal stress τ_{xx} in the transverse direction, (b) the normal stress τ_{yy} in the flow direction, (c) shear stress τ_{xy} and (d) the elastic potential W.

The viscoelastic model, Eq.(1) employed in this computation allows instantaneous elastic response due to the absence of the Newtonian viscous term, and thus we can expect abrupt relaxation of the accumulated elastic energy near expansion.

In Fig. 10 the stress and elastic potential profiles are shown as functions of y (the flow direction) at $x = 1$ (scaled with H_0). Thus they change their domain from the liquid to the solid wall at y=-0.5 and from the solid wall to the liquid at y=0.5, and thus the point in $-0.5 \le y \le 0.5$ means the location at the constriction channel wall. The sharp variation of solutions at $y = \pm 0.5$ clearly demonstrates singular behavior of the solutions incurred by the corners. Especially for τ_{xx} and W, the singular behavior is more intense at the exit corner than that at the entrance corner, which explains severer difficulty present in the constriction flow modeling than in the contraction flow computation. Hence when we search for the convergence limit in these contraction and constriction flow geometries, this difficulty may induce earlier numerical failure in the constriction flow when the result is interpreted with the measure of the Deborah number. We again examine the tendency that the peaks of the stress variables near the corners ($y = \pm 0.5$) become sharper as the mesh becomes finer, and it suggests appropriate mesh convergence of the solutions.

Fig. 11 shows dependence of the streamlines on the flow rate in the neighborhood of the constriction channel for Mesh-B5. In the case of low Deborah number (Fig. 11a), the streamlines in the upstream and the downstream exhibit almost symmetric pattern that corresponds to the linear viscoelastic behavior of the equations. However when the flow rate becomes high ($De > 1$), nonlinearity present in the set of equations dominates, and thus the symmetry breaks. As a result, the vortex size in the downstream decreases whereas that in the upstream increases. The similar dependence of the vortex size on the flow rate has been already obtained by Szabo *et al.* (1997) for the flow through a constriction tube with corner rounding. Evidently the increase of the upstream vortex size with the flow rate results from the same origin with the case of the contraction flow. However elastic recovery of the liquid through sudden expansion similar to the phenomenon in extrudate swelling is thought to result in the decrease of the downstream vortices with the increase of the Deborah number. In other words, when the flow rate is high, the accumulated elastic deformation is large which abruptly relaxes at the exit of constriction, and thus expansion of the liquid due to the relaxation of elastic deformation suppresses the downstream vortex. One can also find deflection of streamlines near the expansion corner when the Deborah number becomes higher than 1.

In the case of finest spatial discretization (Mesh-B5), the normal and shear stresses and the elastic potential have been depicted in Fig. 12. Again one can explicitly see high solution gradient near the corners. However the singularity effect of the expansion corner is much greater than that of the contraction corner. Immediately after the exit of constriction channel, all the viscoelastic variables suddenly relax almost completely. From this we can conclude that numerical interpolation of viscoelastic flow variables near the expansion is much harder than that near the contraction, and this presents another evidence for lower convergence limit in the case of constriction flow modeling.

In order to examine more carefully the flow behavior near the expansion corner, Fig. 13 presents enlarged view of the domain with streamlines for 3 types of spatial discretization such as Mesh-B3, Mesh-B4 and Mesh-B5. In the case of Mesh-B3 where the finest corner element has $0.025H_0$ as its side length, only the streamlines almost parallel to the wall are observed. However when the flow domain becomes more finely discretized (Fig. 13b-c), we see occurrence of small lip vortex just before the exit to expansion, which seems to be responsible for the deflection of streamlines near the exit corner. It is worthwhile to emphasize once more that this type of lip vortex can be numerically obtained only when the spatial discretization is fine enough, and it becomes more distinct when the mesh is more refined. Whereas the occurrence of the lip vortex

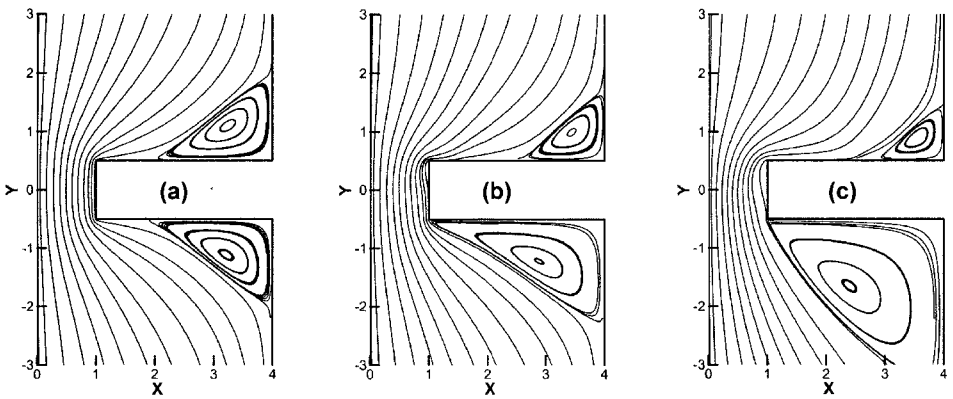

Fig. 11. Streamlines of 4:1:4 constriction flow for Mesh-B5 at (a) $De = 0.2$, (b) $De = 2$ and (c) $De = 10$.

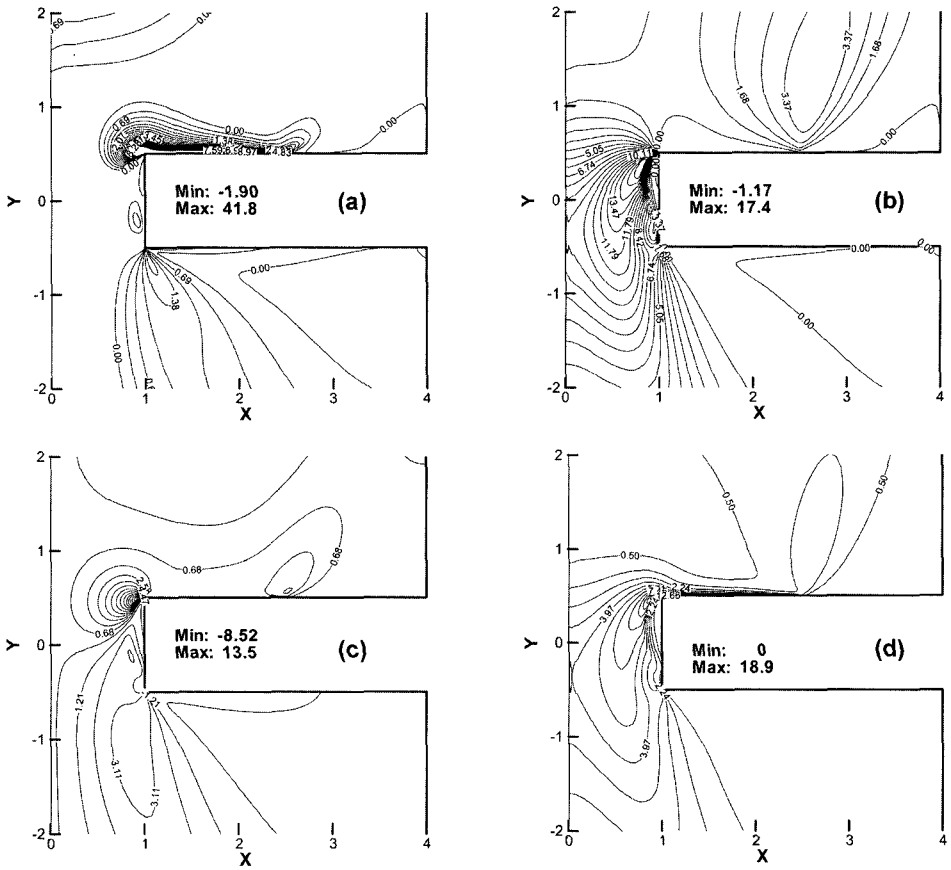

Fig. 12. Contourlines of normal stresses (a) in the transverse direction (τ_{xx}) and (b) in the flow direction (τ_{yy}), (c) shear stress (τ_{xy}) and (d) elastic potential (W) of 4:1:4 constriction flow at $De = 10$ for Mesh-B5.

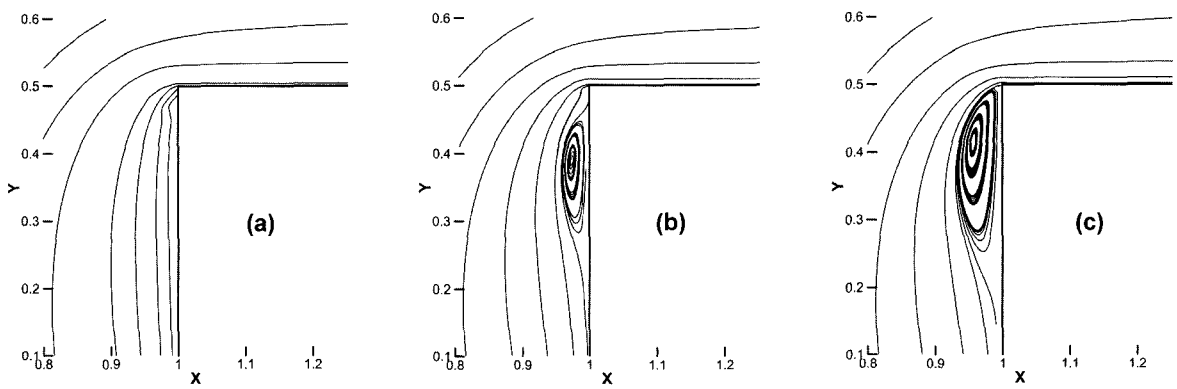

Fig. 13. Streamlines of 4:1:4 constriction flow at $De = 10$ near the exit corner for (a) Mesh-B3, (b) Mesh-B4 and (c) Mesh-B5.

actually makes narrower the width of the channel near the constriction exit, it plays a role similar to the corner rounding and thus smoothens bending of the streamlines at the exit corner.

Before concluding this chapter, we make a remark on the accuracy issue regarding the employment of logarithmic variables instead of original viscoelastic variables. At first sight, one may consider that numerical interpolation of the logarithmically transformed variables brings about loss of accuracy, since the logarithmic transform converts the exponential scale into the linear one. However it actually preserves consistency in the numerical interpolation. To illustrate this, we only consider the simple case of 2D planar situation with the Leonov model. In this case, when we denote the first unknown eigenvalue of the $\boldsymbol{c}$ tensor as c, the second one becomes $1/c$, since both the third eigenvalue and the determinant of $\boldsymbol{c}$ are unit. Thus the domain of (0, 1] is exactly equivalent to the domain of [1, ∞) from

the viewpoint of eigenvalues of $\boldsymbol{c}$. Therefore the direct interpolation of the $\boldsymbol{c}$ tensor variables by polynomials provides insufficient accuracy in (0, 1], even though it gives highly accurate approximation in [1, ∞). However the logarithmic transform converts the domain of (0, 1] into (-∞, 0] and [1, ∞) into [0, ∞). Thus only the logarithmically transformed variables can be interpolated equivalently in the whole domain. As a result, the tensor-logarithmic formulation provides consistent and equivalent numerical interpolation of the viscoelastic variables in their whole domain in addition to the advantage that it preserves the positive-definiteness of the configuration tensor.

6. Conclusions

In this work, planar 4:1 contraction and 4:1:4 contraction/expansion viscoelastic flows are analyzed in terms of finite element method with tensor-logarithmic formulation of the configuration tensor implemented. The isothermal incompressible creeping viscoelastic flows with the Leonov model are considered. We have obtained solutions over the Deborah number of 100 for the contraction flow and over 10 for the constriction flow. In both cases, there seems to exist slight decrease of convergence limit as the mesh becomes finer. From this analysis, singular behavior of the sharp corners has been clearly demonstrated and proper interpolation of variables in terms of the logarithmic transformation is explained. In the case of the constriction flow, the exit corner imposes much severer singularity than the entrance corner. In addition, the upstream vortex increases but the downstream vortex decreases in their size as the flow rate increases. When the spatial resolution is fine enough and the Deborah number is high, the deflection of the streamlines just before the constriction exit is found, and small lip vortex has been observed. This small vortex seems to occur due to abrupt expansion of the elastic liquid through the constriction exit that accompanies sudden relaxation of elastic deformation.

Acknowledgements

This work was supported by the Korea Research Foundation Grant funded by the Korean Government (MOE-HRD) (KRF-2004-0105-000).

References

Fan, Y., R. I. Tanner and N. Phan-Thien, 1999, Galerkin/least-square finite-element methods for steady viscoelastic flows, *J. Non-Newtonian Fluid Mech.* **84**, 233-256.

Fattal, R. and R. Kupferman, 2004, Constitutive laws of the matrix-logarithm of the conformation tensor, *J. Non-Newtonian Fluid Mech.* **123**, 281-285.

Guenette, R. and M. Fortin, 1995, A new mixed finite element method for computing viscoelastic flows, *J. Non-Newtonian Fluid Mech.* **60**, 27-52.

Gupta, M., 1997, Viscoelastic modeling of entrance flow using multimode Leonov model, *Int. J. Numer. Meth. Fluids* **24**, 493-517.

Hulsen, M. A., 2004, Keynote presentation in Internatioan Congress on Rheology 2004, Seoul, Korea.

Hulsen, M. A., R. Fattal and R. Kupferman, 2005, Flow of viscoelastic fluids past a cylinder at high Weissenberg number: Stabilized simulations using matrix logarithms, *J. Non-Newtonian Fluid Mech.* **127**, 27-39.

Kwon, Y., 2004, Finite element analysis of planar 4:1 contraction flow with the tensor-logarithmic formulation of differential constitutive equations, *Korea-Australia Rheology J.* **16**, 183-191.

Kwon, Y. and A. I. Leonov, 1995, Stability constraints in the formulation of viscoelastic constitutive equations, *J. Non-Newtonian Fluid Mech.* **58**, 25-46.

Leonov, A. I., 1976, Nonequilibrium thermodynamics and rheology of viscoelastic polymer media, *Rheol. Acta* **15**, 85-98.

Szabo, P., J. M. Rallison and E. J. Hinch, 1997, Start-up of flow of a FENE-fluid through a 4:1:4 constriction in a tube, *J. Non-Newtonian Fluid Mech.* **72**, 73-86.